Quadrupole method: A new approach for solving the direct problem of electrical resistance tomography

Fatma Ouled Saad, Aymen Sdayria, Jamel Madiouli, Jalila Sghaier, Olivier Fudym

King Saud University

Journal of King Saud University – Science

Quadrupole method: A new approach for solving the direct problem of electrical resistance tomography

CrossMark

Fatma Ouled Saad [a,*], **Aymen Sdayria** [b], **Jamel Madiouli** [a,c], **Jalila Sghaier** [a], **Olivier Fudym** [d]

[a] *U.R. Thermique et thermodynamique des procédés industriels, National Engineering School of Monastir, E.N.I.M, University of Monastir, Tunisia*
[b] *Laboratoire d'Energétique et des Transferts Thermiques et Massique, LETTM, FST, University of Tunis Al-Manar, Tunisia*
[c] *Faculty of Engineering, King Khalid University, Abha, Saudi Arabia*
[d] *RAPSODEE CNRS École des Mines d'Albi, University of Toulouse, France*

Abstract An inverse problem was considered to estimate electrical conductivity distribution for the electrical resistance tomography. This technique allows to control the internal parameters by reconstructing the distribution of electrical conductivity of liquid/solid suspension. As an analytical tool, the quadrupole method was used to solve the forward problem in order to simulate the sensors voltage evolution. The inverse problem is solved using the Levenberg–Marquardt method. A major source of uncertainty in tomographic inversion is the data error. The effect of the measurement errors on the stability of the solution was investigated. In order to find the current injection strategy which gives more information about the electrical conductivity, sensitivity analysis was carried out.

The effect of Levenberg–Marquardt coefficient and initial value of the conductivity on the stability of the scheme was analyzed. The developed algorithm can be employed to rebuild the electrical conductivity which permits to go back to the physical parameters of the suspension.

1. Introduction

Electrical resistance tomography (ERT) is a nonintrusive technique that determines the conductivities of different materials. The task of image reconstruction for ERT is to estimate the electrical conductivity distribution from voltage measurements.

Because of its advantages, Electrical tomography is widely used in environmental applications where the direct current (DC) resistivity surveying was applied to a number of example sites (Dahlin, 1996; Dahlin and Zhou, 2004; Zhou and Dahlin,

ELSEVIER **Production and hosting by Elsevier**

Nomenclature

A, B, C, D	generalized quadrupole matrices
A_e	area of electrode [m^2]
d	elements of the diagonal matrix Ω
e	thickness [m]
F	current flux density
H	hessian matrix
i	ith grid
i^+, i^-	ith grid interfaces
I	electrical current [A]
J	jacobian matrix
$\mathbb{K}$	electrical conductivity diagonal matrix
L	length [m]
$\mathbb{M}$	diagonal matrix
M	measurement number
N	nodes number with respect to z
n	the vector normal to the surface
O_b	objective function
R	voltage vector in the diagonal basis
r	elements of the voltage vector in the diagonal basis
T	eigenvectors matrix
U	voltage [V]
V	potential [V]
x, z	geometric variables [m]

z_1	position of the source electrode
z_2	position of the sink electrode
Δz	space step [m]
σ	electrical conductivity [S/m]
$\o$	current flux density [A/m^2]
Ω	diagonal matrix
II	identity matrix
λ	Levenberg–Marquardt coefficient.
ζ	relative error

Subscripts

cal	calculated value
exact	exact value
k	kth element
m	measured value
R	relative to eigenvalue basis

Superscripts

0	initial value
l	iteration number
t	transpose of matrix

2003; Sasaki, 1992). In geophysics, this technique is used to represent changes in soil electrical resistivity (Dahlin, 2001).

The electrical tomographic methods applied in two-phase flow measurement have become popular (Dong et al., 2003; Wang, 2000; Ma et al., 2001; Lucas et al., 1999). In the same field, Giguère et al. (2008a,b) has worked on image reconstruction for bi-dimensional ERT to visualize multiphase flow.

Wang et al. (1999) used an ERT system to measure the gas–liquid mixture in a stirred vessel (Giguère et al., 2008a,b). Ma et al. (2001) were interested in the application of ERT in horizontal pipes of gas and liquid flow. Lucas et al. (1999) used this technique to monitor conductivity in vertical pipes and other inclined. Electrical resistance tomography has already been applied for imaging of flotation process (Wang et al., 1999; Nissinen et al., 2014; Cilliers et al., 1999; Kourunen et al., 2008; Normi et al., 2009; Lehikoinen et al., 2011). This technique measures solids concentration profile and stability in the hydrocyclones (Williams et al., 1995; Reunanen et al., 2011; Hua et al., 1987; Abdullah et al., 1993; Bond et al., 1999). Binley et al. (1996) applied this technique in the environmental field in order to detect leakage from nuclear waste storage tanks. It was also used in multiplane imaging of mixers (Mann et al., 1995). In the same field, it was applied in the quantification of the homogeneity of mixing (Rosales et al., 2012).

In the processing of suspension, the application of a nonintrusive technique is important since the particle volume-fraction distribution has an effect on the rheological properties. Also the concentration is necessary for understanding industrial processes. In this context, Kim et al. (2004) proposed an algorithm of the Electrical Impedance Tomography (EIT) for particle concentration distribution in suspension.

To control and optimize some industrial sedimentation processes, Tossavainen et al. (2007) introduces a new computational method for sedimentation monitoring using electrical impedance tomography (EIT).

Many industrial processes present a layered materials distribution which needs to be solved in a rectangular configuration. In this context, Ren et al. (2013) was interested in the problems where the permittivity is piecewise constant.

One of the benefits of the electrical methods is that no transparent processes tanks are needed to control the internal phenomena (Tossavainen et al., 2007). Electrical tomography techniques are known by its good portability, high speed, and low cost.

The technique of ERT consists of applying a direct current between two electrodes and measuring the electrical voltage between two others. The voltage depends on the electrical conductivity of the medium between the electrodes. In terms of mathematics, the ERT image reconstruction is a non linear inverse problem. It includes iteratively solving forward and inverse problems (Kim et al., 2014).

Currently, the ERT forward problem solvers are mainly based on finite element method (FEM), which requires a large number of mesh elements (Xu and Dong, 2010; Hallaji and Pour-Ghaz, 2014; Liu et al., 2014). Although FEM is the natural choice for several simulations (Tossavainen et al., 2007), modeling of thin layers, involves serious compromise in accuracy and robustness (Das et al., 2006).

Brebbia et al. (1991) confirmed that FEM is inefficient to use in many engineering applications. The Boundary Element Method (BEM) (Xu et al., 2010; Khambampati et al., 2012; Ren et al., 2013) is widely used to solve the forward problem necessitating a simple inversion of a linear system. This

method transforms the domain into boundary problem (Xu and Dong, 2010). It needs to discretize just the boundaries of the domain, which save memory space and computation time. BEM is applicable to complex engineering problems. However, conventional BEM formulation suffers from accuracy if geometric discontinuities are present along the boundary (Das et al., 2006).

In the present study, a new method was proposed based on the quadrupole technique applied to electrical fields for numerical resolution of the forward problem Nevertheless; the boundary-element method exhibits some similarities to the quadrupole formalism, provided that for both techniques the state variables and flux are calculated first on the boundaries, and not necessarily on the entire domain (Khambampati et al., 2012).

Generally, the quadrupole method has been used in heat transfer modeling (Fudym et al., 2002, 2007; Pailhes et al., 2012; Degiovanni, 1988). It represents an analytical tool which consists in assembling multilayered slabs with different geometrical and thermophysical properties. Fudym et al. (2002) investigated the problem of finding a generalized intrinsic relationship between temperature and heat flux at the boundaries of a heterogeneous medium with one-dimensional varying properties in the layer direction. In this paper, quadrupole method was adopted to simulate the sensor voltage evolutions created by the current injection through electrodes placed along the boundaries of a heterogeneous medium.

Solving the forward problem supports a sensitivity analysis in order to know the most appropriate injection strategies. The inverse problem for the ERT is solved in order to estimate the electrical conductivity which is necessary to predict many parameters such as volume fraction and suspension concentration. The inverse problem is non-linear, an image reconstruction algorithm is necessary (Batsale et al., 1994). The Levenberg–Marquardt (LM) (Moré, 1978; Xie et al., 1995; Fguiri et al., 2013) technique was adopted to solve the inverse problem. It offers fast convergence attempting to find the local minimum nearest to the starting point. The proposed method in this study is evaluated with simulated measurement obtained by adding an error to the calculated voltage. The stability of the LM method is analyzed. The influence of the injection electrode position (measurement strategies), the initial value of the estimated conductivity, the relative error and the LM parameter on the estimations are also investigated.

2. Models

The ERT problem resolution aims to reconstruct the electrical conductivity spatial distribution. This is accomplished by measuring the electrode potentials at the boundaries of the object under the influence of an applied current. The current is applied between different pairs of electrodes and the resulting electrical potential differences across the remaining pairs of electrodes are measured. The reconstruction of the conductivity distribution from the applied current and measured voltages requires a physical model named as forward problem which describes the dependence of the potentials at the boundaries to the conductivity distribution.

In this numerical study, the quadrupole method is applied to electrical fields in order to solve the forward problem. Levenberg–Marquardt method is used as an inverse solver to estimate the unknown electrical conductivity from the measured boundary voltages. Numerical and phantom experiments are performed to validate the performance of the proposed method.

As can be seen in Fig. 1, the computational domain is restricted to the vertical plane of a cylindrical cell. 10 equidistant electrodes are placed at the boundary of this plane, 5 by each side. Each electrode from those numbered from 1 to 5 will be considered as a cathode for the current injection. Electrodes of the other side will be considered as anodes. The model is characterized in two parts. The forward problem and the inverse are presented below.

2.1. Forward problem

The forward problem of the ERT is solved in two-dimensional configuration. It consists in finding the electrical potential distribution V with a known electrical conductivity distribution (σ) and current flow density I/Ae.

The governing equations are established assuming that:

- A bidimensional medium (L = 0.1 m, e = 0.3 m) was considered for different numerical tests.
- The electrical conductivity changes with respect to z.

The mathematical model of the ERT is defined by the tomography equation which derives from Maxwell equations:

$$\nabla \cdot (\sigma(z)\nabla V(x, z)) = 0 \tag{1}$$

And the following boundary conditions

$$\sigma \partial V / \partial n = -I/A_e \text{ on the cathode;} \tag{2}$$

$$\sigma \partial V / \partial n = I/A_e \text{ on the anode;} \tag{3}$$

$$\sigma \partial V / \partial n = 0 \text{ on insulating surface} \tag{4}$$

where n is the normal vector to the surface.

The quadrupole method is a well-known analytical tool in heat transfer modeling in heterogeneous samples or non-uniform convective heating in the context of Non-Destructive thermal Evaluation. This method allows to assemble multilayered slabs with different geometrical and thermophysical properties (Fudym et al., 2002).
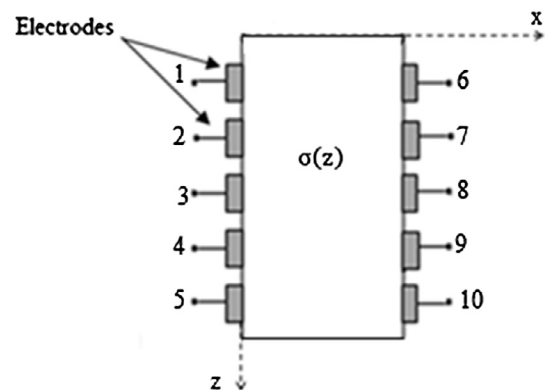

Figure 1   Electrodes Model.

The quadrupole general theory consists in finding a generalized intrinsic relationship between potential and current flux at the boundaries of the medium to study. This relationship is defined by a matrix that relates the input and the output after an integral space transform. The main advantage of this relationship is to make easy the representation of multilayered system by multiplying the corresponding quadrupole matrices (Fudym et al., 2002).

The forward problem is defined by the tomography equation:

$$\sigma(z)\frac{\partial^2 V(x,z)}{\partial x^2} + \frac{\partial}{\partial z}\left(\sigma(z)\frac{\partial V(x,z)}{\partial z}\right) = 0 \tag{5}$$

The boundary conditions are defined as:

- $z = 0 \Rightarrow \sigma(0)\dfrac{\partial V}{\partial z} = 0$ (6)

- $z = e \Rightarrow \sigma(e)\dfrac{\partial V}{\partial z} = 0$ (7)

- $x = 0$ (8)

  $\checkmark\quad 0 < z < z_1 \Rightarrow -\sigma(z)\dfrac{\partial V}{\partial x} = 0$

  $\checkmark\quad z = z_1 \Rightarrow -\sigma(z_1)\dfrac{\partial V}{\partial x} = I/A_e$

  $\checkmark\quad z_1 < z < e \Rightarrow -\sigma(z)\dfrac{\partial V}{\partial x} = 0$

- $x = L$ (9)

  $\checkmark\quad 0 < z < z_2 \Rightarrow -\sigma(z)\dfrac{\partial V}{\partial x} = 0$

  $\checkmark\quad z = z_2 \Rightarrow -\sigma(z_2)\dfrac{\partial V}{\partial x} = -I/A_e$

  $\checkmark\quad z_2 < z < e \Rightarrow -\sigma(z)\dfrac{\partial V}{\partial x} = 0$

To solve this set of obtained algebraic equations, space discretization of Eqs. ((5)–(9) is performed versus the z direction (Fig. 2). N new variables are introduced as

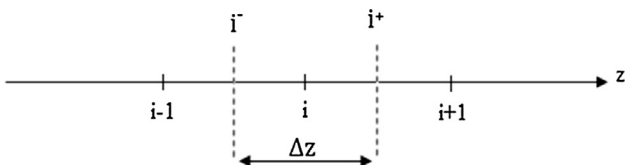$$V_i = V_i(x) = \frac{1}{\Delta z}\int_{i^-}^{i^+} V(x,z)\,dz$$

where i defines the ith element of the potential vector V with respect to z.

i^+ and i^- indicate the ith gird interfaces.

Thermal quadrupole formalism (Fudym et al., 2002) is adopted (Fig. 3). The input and output variables in terms of electrical potential and the electrical current flux are connected by the following relationship:

$$\begin{bmatrix} V \\ \emptyset \end{bmatrix}_0 = \begin{bmatrix} A & B \\ C & D \end{bmatrix}\begin{bmatrix} V \\ \emptyset \end{bmatrix}_L$$

where A, B, C and D are a matrix found using Quadrupole formalism.

V(0) and V(L) are defined as the potential vectors (with respect to z) at the positions x = 0 and x = L. As the same ø(0) and ø(L) are the electrical current flux vectors (with respect to z) at the positions x = 0 and x = L.

Eqs. (5)–(9) are then integrated relative to z:

$$\sigma_i\Delta z\frac{\partial^2 V_i}{\partial x^2} + \varphi_{i^-} - \varphi_{i^+} = 0 \tag{10}$$

where σ_i is the ith element of the vector σ defined as:

$$\sigma = [\sigma(z_i)] = [(\sigma_i)];\, i = 1, N$$

and

$$\varphi_{i^-} = P_{i^-}[V_{i-1} - V_i]$$

$$\varphi_{i^+} = P_{i^+}[V_i - V_{i+1}]$$

$$P_{i^-} = \left[\frac{\Delta z}{2\sigma_{i-1}} + \frac{\Delta z}{2\sigma_i}\right]^{-1}$$

$$P_{i^+} = \left[\frac{\Delta z}{2\sigma_i} + \frac{\Delta z}{2\sigma_{i+1}}\right]^{-1}$$

$$\sigma_i\Delta z\frac{\partial^2 V_i}{\partial x^2} + P_{i^-}V_{i-1} - [P_{i^+} + P_{i^-}]V_i + P_{i^+}V_{i+1} = 0 \tag{11}$$

Both boundary conditions at z = 0 and z = e are expressed in the same way in order to obtain the corresponding equations at node i = 1 and i = N.

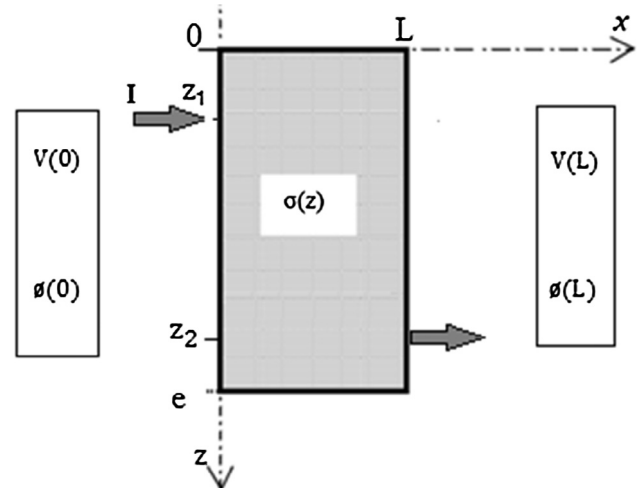**Figure 2** Discretization with respect to z.

Figure 3 ERT model.

For the boundary conditions ($z = 0$) and ($z = e$), the equations are:

$$\sigma_1 \Delta z \frac{\partial^2 V_1}{\partial x^2} + P_{1^+} V_1 - P_{1^+} V_2 = 0 \tag{12}$$

$$\sigma_N \Delta z \frac{\partial^2 V_N}{\partial x^2} - P_{N^-} V_N + P_{N^-} V_{N-1} = 0 \tag{13}$$

These Eqs. (11)–(13) can be written in matrix form as:

$$\mathbb{K}^{-1} \mathbb{M} V - \frac{d^2 V}{dx^2} = 0 \tag{14}$$

where V is a vector of the N potentials at the position x.

$$V = [V_1 V_2 \ldots V_N]^t$$

$$\mathbb{K} = \text{diag}[\sigma_1 \Delta z \ \sigma_2 \Delta z \ldots \sigma_N \Delta z]$$

$$\mathbb{M} = \begin{bmatrix} P_{1^+} & -P_{1^+} & 0 & & & & \\ -P_{2^-} & P_{2^-} + P_{2^+} & -P_{2^+} & & & & \\ 0 & -P_{3^-} & P_{3^-} + P_{3^+} & -P_{3^+} & 0 & & \\ & & \ldots & & \ldots & \ldots & \\ & & & -P_{i^-} & P_{i^-} + P_{i^+} & -P_{i^+} & \\ & & & \ldots & \ldots & \ldots & \\ & & & & & -P_{N^-} & P_{N^-} \end{bmatrix}$$

where the operator "diag" is used in order to build a diagonal matrix from the corresponding vector.

The term $\mathbb{K}^{-1} \mathbb{M}$ is x independent, Eq. (14) can be solved directly by the diagonalization of this matrix.

So its diagonalization gives:

$$\mathbb{K}^{-1} \mathbb{M} = T \Omega T^{-1} \tag{15}$$

where Ω: diagonal matrix considering a change of variables $R = T^{-1} V$ where R is the potential vector in the new basis.

Eq. (14) becomes

$$T \Omega T^{-1} V - \frac{d^2 V}{dx^2} = 0$$

Introducing the potential vector (R), the precedent equation can be written

$$T \Omega R - T \frac{d^2 R}{dx^2} = 0$$

$$\Omega R - \frac{d^2 R}{dx^2} = 0 \tag{16}$$

It has seen that in the Eq.(16), only the unknown vector R is x-dependent. The expression is a second order ordinary differential diagonal system.

Each line of Eq. (16) is

$$\frac{d^2 r_k}{dx^2} - d_k r_k = 0$$

where r_k is the kth element of the vector R. d_k is the kth diagonal coefficient of the matrix Ω.

The general solution of this equation has the form

$$r_k = G_1 E_1(x) + G_2 E_2(x) \tag{17}$$

where $E_1 = \cosh(\sqrt{d_k} x)$ and $E_2 = \sinh(\sqrt{d_k} x)$

G_1 and G_2 are constants, these constants are calculated using the boundary conditions at $x = 0$ and $x = L$:

$$G_1 = r_k(0)$$

and

$$G_2 = [r_k(L) - r_k(0) \cosh(\sqrt{d_k} L)] \frac{1}{\sinh(\sqrt{d_k} L)}$$

In order to find a linear relationship between the potential and current flux (Fudym et al., 2002), scalar quadrupole formalism is developed by introducing the integration constants G1 and G2 in Eq. (16). Introducing the flux in the eigenvalues basis:

$$f_k = -\frac{dr_k}{dx}$$

The scalar quadrupole at $x = 0$ and $x = L$ location is written as:

$$\begin{bmatrix} r_k \\ f_k \end{bmatrix}_0 = \begin{bmatrix} A_k & B_k \\ C_k & D_k \end{bmatrix} \begin{bmatrix} r_k \\ f_k \end{bmatrix}_L \tag{18}$$

where A_k, B_k, C_k, D_k are scalar terms of the quadrupole

$$A_k = \cosh(\sqrt{d_k} L)$$

$$B_k = \sinh(\sqrt{d_k} L)(\sqrt{L})^{-1}$$

$$C_k = (\sqrt{L}) \sinh(\sqrt{d_k} L)$$

$$D_k = \cos h(\sqrt{d_k} L)$$

In the vector form the quadrupole can be implemented using vector R of (r_k) and introducing the flux F_R as

$$F_R = -\frac{dR}{dx}$$

This can be written

$$\begin{bmatrix} R \\ F_R \end{bmatrix}_0 = \begin{bmatrix} A_R & B_R \\ C_R & D_R \end{bmatrix} \begin{bmatrix} R \\ F_R \end{bmatrix}_L \tag{19}$$

A_R, B_R, C_R and D_R are diagonal matrices built with the scalar terms corresponding to Eq. (18)

$$A_R = \cosh(\sqrt{\Omega} L)$$

$$B_R = \sinh(\sqrt{\Omega} L)(\sqrt{\Omega})^{-1}$$

$$C_R = (\sqrt{\Omega}) \sinh(\sqrt{\Omega} l L)$$

$$D_R = \cosh(\sqrt{\Omega} L)$$

The current flux density vector ø is written as

$$ø = -\mathbb{K} \frac{dV}{dx}$$

The relationship between F_R and ø is:

$$ø = \mathbb{K} T F_R$$

The Eq. (19) is a generalized quadrupole in terms of the potential and the current flux density such as:

$$\begin{bmatrix} T^{-1} V \\ (\mathbb{K} T)^{-1} ø \end{bmatrix}_0 = \begin{bmatrix} A_R & B_R \\ C_R & D_R \end{bmatrix} \begin{bmatrix} T^{-1} V \\ (\mathbb{K} T)^{-1} ø \end{bmatrix}_L \tag{20}$$

So

$$\begin{bmatrix} V \\ \emptyset \end{bmatrix}_0 = \begin{bmatrix} A & B \\ C & D \end{bmatrix} \begin{bmatrix} V \\ \emptyset \end{bmatrix}_L \qquad (21)$$

where

$$A = TA_R T^{-1}$$

$$B = TB_R(\mathbb{K}T^{-1})$$

$$C = \mathbb{K}TC_R T^{-1}$$

$$D = \mathbb{K}TD_R(\mathbb{K}T)^{-1}$$

In our problem the current flux density ø(0) at x = 0 and ø(L) at x = L are known, it can deduced V(0) andV(L) from the generalized quadrupole:

$$V(L) = C^{-1}\emptyset(0) - C^{-1}D\emptyset(L) \qquad (22)$$

$$V(0) = AV(L) + B\emptyset(L) \qquad (23)$$

2.2. Inverse problem

Solving the inverse problem consists in minimizing the difference between the numerical simulated voltages and the physical reality represented by the experimental ones defined in an objective function (O_b).

It is to identify the vector of parameters σ that minimizes the sum of squares function written as:

$$O_b(\sigma) = (U_m - U_{cal}(\sigma))^T(U_m - U_{cal}(\sigma)) \qquad (24)$$

where σ is the electrical conductivity which depends on z, and U is the vector of electrical voltages. Subscripts m and cal represent measured and calculated values. For the measurements, the simulated experimentations were used.

The problem is non-linear, which requires a method of iterative programing. The Levenberg–Marquardt method was applied.

The iterative procedure of the Levenberg–Marquardt method is given by:

$$\{\sigma\}^{l+1} = \{\sigma\}^l - ([H + \lambda.II]^{-1})^l\left\{(J^l)^t(U_m - U_{cal}(\sigma^l))\right\} \qquad (25)$$

where J is the jacobian matrix containing the partial derivatives of $U_{cal,i}$ (i = 1, M) with respect of the parameters to be estimated. The coefficient of the Jacobian matrix is defined as

$$J_{ij} = \frac{U_{cal,i}(\sigma_1, \sigma_2, ..., \sigma_j + \partial\sigma, ..., \sigma_N) - U_{cal,i}(\sigma_1, ..., \sigma_j, ..., \sigma_N)}{\sigma_j\partial\sigma}$$

λ is a damping parameter (Marquardt parameter) added to the diagonal of the approximated hessian matrix ($H = J^tJ$) in order to control the stability of the algorithm.

$U_{cal,i}$ is the ith element of the calculated voltage vector U_{cal} defined as:

$$U_{cal} = [U_{cal,1} U_{cal,2} ...... U_{cal,M}]$$

and $U_{m,i}$ is the ith element of the measured voltage vector U_m defined as:

$$U_m = [U_{m,1} U_{m,2} ...... U_{m,M}]$$

Iterations are generally started with large values of the damping parameter. Then this parameter is gradually reduced as the solution approaches the converged result.

3. Electrical injection strategies

For all types of geometry, ERT systems are designed such that the current is injected into the object through a pair of electrodes and voltages are measured using other pairs. An electrical current source requires switches that choose electrodes for current injection.

In most applications, the ERT is used to reconstruct the conductivity spatial distribution in a disk. Generally, the adjacent strategy is used for ERT data acquisition (Seagar et al., 1987; Dickin and Wang, 1996; Giguère et al., 2008a,b; Nissinen et al., 2014). In the adjacent strategy, current distribution is non-uniform due to most of the current travels near the peripheral electrodes (Xu and Dong, 2010). This will cause high interference of measurement error and noise due to the lower current density at the center of the vessel. However, this method is widely used for ERT data acquisition in a disk, due to its minimal hardware capacity. Besides, image reconstruction can be done relatively fast.

Compared to the adjacent strategy used in disks, diagonal method has the benefit of better sensitivity over the entire disk and is not sensitive to measurement error and thus produces better quality but has a disadvantage of lower sensitivity in the periphery.

In this paper, the reconstruction of electrical conductivity distribution is made in the vertical plane of a cylindrical cell. Different injection strategies, applied to a rectangular configuration, are compared. Such an electrode configuration may be desirable for using electrical resistance tomography in the case where physical parameters are changing with respect to z in cylindrical vessels.

In order to establish a sensitivity analysis of the model, a comparison between 3 different configurations of current injection was considered to determine the most sensitive.

As shown in Figs. 1 and 10 electrodes are placed in the vertical plan, 5 by each side. The electrical conductivity was assumed constant in a horizontal plan.

The adjacent strategy (Fig. 4), consists in applying the current through two neighboring electrodes and the voltage is measured successively from all other adjacent electrode pairs [26]. Current (I) is then applied through the next pair of electrodes and the voltage measurements are repeated.

First, the current is injected between the electrodes 1 and 2, voltages (U) are measured successively between all other pairs of adjacent electrodes (3–4), (4–5), (5–10), (10–9), (9–8), (8–7), and (7–6), and then the current is injected between 3 and 4. Voltages are measured between the pairs of electrodes (1–2), (2–5), (5–10), (10–9), (9–8), (8–7), and (7–6). The procedure is repeated until all the independent measurements have been made. The number of independent measured voltages is 35.

The second configuration (shown in Fig. 5) corresponds to the opposite strategy. The current is applied through two opposed electrodes. The other pairs of opposed electrodes are used to measure the voltage. The next set of data is obtained by switching the current to the next pair of electrodes.
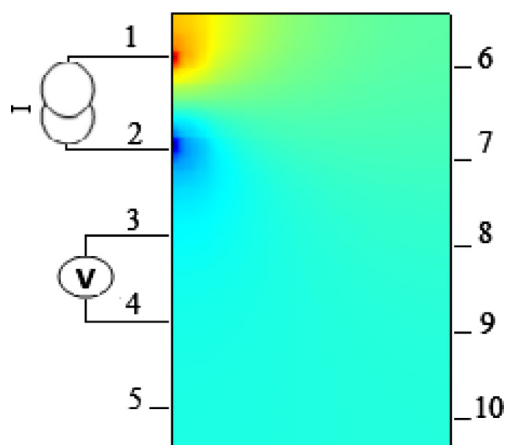
Figure 4   Strategy of adjacent electrodes.

The current is applied between the electrodes 1 and 6, voltages are measured successively between all other pairs of opposite electrodes (2–7), (3–8), (4–9) and (5–10). Then the current is injected between 2 and 7. Voltages are measured between the pairs of electrodes (1–6), (3–8), (4–9) and (5–10). The procedure is repeated until all the opposite electrodes have been used as a source of current.

The third considered configuration (shown in Fig. 6) is the diagonal strategy, where the current is applied through two diagonal electrodes at the peripheries of the plan. The electrode adjacent to the current-injecting one is used as the voltage reference. So, for a particular pair of current-injecting electrodes, the voltages are measured with respect to the reference at all the electrodes except the current-injecting ones.

The current-injecting pair of electrodes is (1–10), then the electrode number 2 is used as reference for voltage measurements (2–3), (2–4), (2–5), (2–6), (2–7), (2–8) and (2–9). Then the current is injected between 2 and 9. The adjacent electrode

(3) is then used as the voltage reference. Voltages are measured between the pairs of electrodes (3–1), (3–4), (3–5), (3–6), (3–7), (3–8) and (3–10). The procedure is repeated until all the opposite electrodes have been used as a source of current. So, 35 measured voltages were obtained.

4. Sensitivity analysis

Before starting the identification, a sensitivity analysis should be carried out in order to choose the current injection strategy that gives more information on the electrical conductivity distribution in rectangular configuration. The elements of the Jacobian matrix known as sensitivity coefficients are defined as the first derivative of the variable to be calculated according to the unknown parameters:

$$J_{ij} = \frac{\partial U_{cal,i}(\sigma_j)}{\partial \sigma_j} \quad i = 1 \ldots M$$
$$j = 1 \ldots N$$

The sensitivity coefficients are calculated by the Direct Difference Method.

5. Results and discussion

5.1. Resolution of the forward problem

The resolution of the tomography equation using the quadrupole method applied to electric fields allowed to determine the distribution of electrical voltage in the suspension.

The spatial variation of the electrical potential at the boundaries was traced for different electrical conductivity value by fixing the current flow. According to Fig. 7, it is observed that these two parameters are inversely proportional. The potential, in absolute value, is even higher when the conductivity is lower. Also it has been noticed that this influence decreases for the most conductive environments.
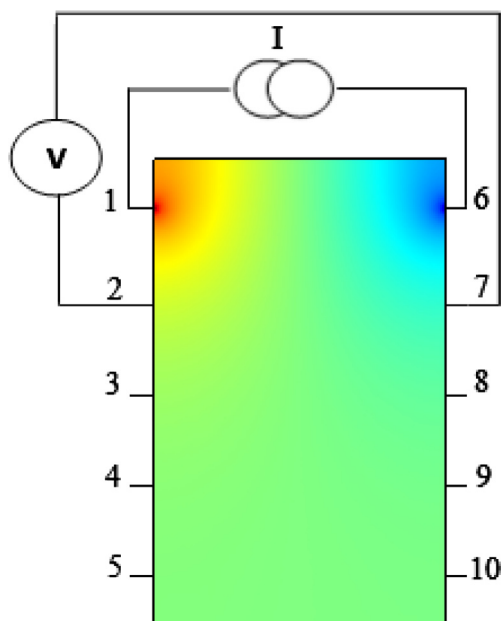

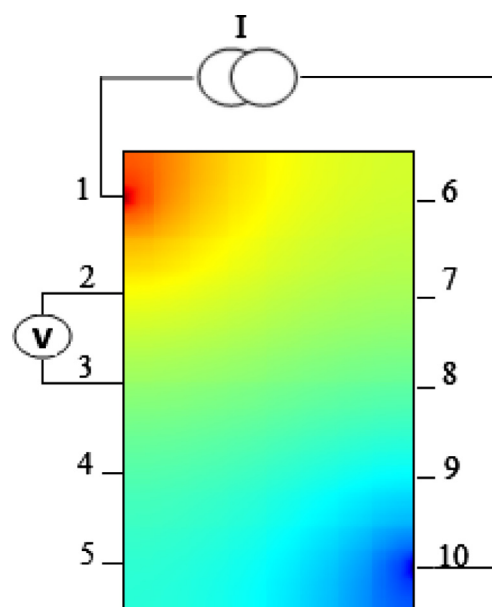**Figure 5**   Strategy of opposite electrodes.

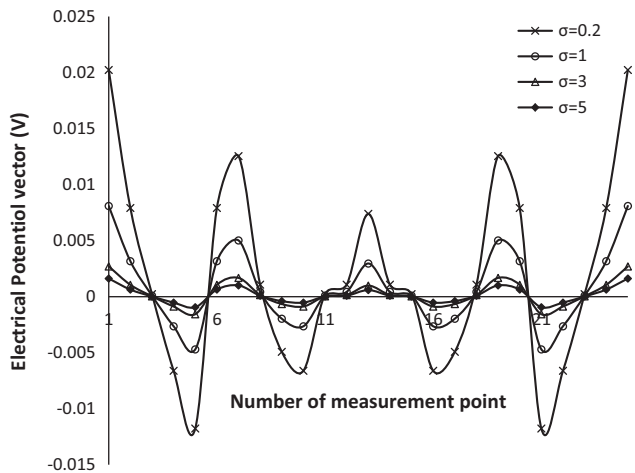**Figure 6**   Strategy of diagonal electrodes.

Figure 7 Spatial variation of the electrical potential at the boundaries for different electrical conductivity value.

The analysis of the sensitivity for different electrical conductivities ($\sigma(z)$) was evaluated. In Fig. 8, the spatial distribution of the sensitivity coefficients for different configurations was illustrated.

The adjacent strategy has a non-uniform current distribution since most of the current density travels near the peripheral electrodes. Therefore, the current density at the center is relatively low which makes the strategy very sensitive to measurement error and noise (Tapp, 2000).

Also for the second strategy of measurement (opposite injection), the most current density travels between the opposite electrodes, which makes the value of the sensitivity coefficient low for most conductivities. Compared to that of the adjacent electrodes, this strategy has a higher sensitivity.

It can be seen that, using the strategy of diagonal electrodes, the model is very sensitive to the electrical conductivity variation in a rectangular configuration.
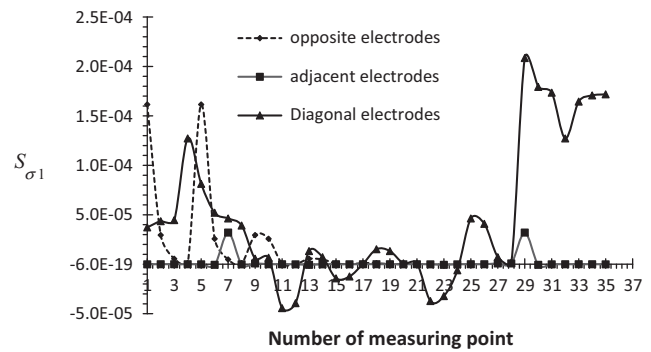
A comparison between three strategies of current injection for different electrical conductivities was performed. Fig. 8-a, b, c illustrate the evolutions of the sensitivity to electrical conductivity of, respectively, the second vertical plane (σ_2), the first plane (σ_1) and the fifth plane (σ_5). For different electrical conductivities, the highest values of reduced sensitivity (in absolute values) are achieved with the diagonal injection strategy. Therefore, the evolution of the relative sensitivity is affected by the position measurement of the voltage and the position of the current injection electrodes. It can be concluded that the third case of current injection (between two diagonal electrodes) has the best current distribution in the rectangular configuration. Also the number of measurements has an influence on the sensitivity of the model.
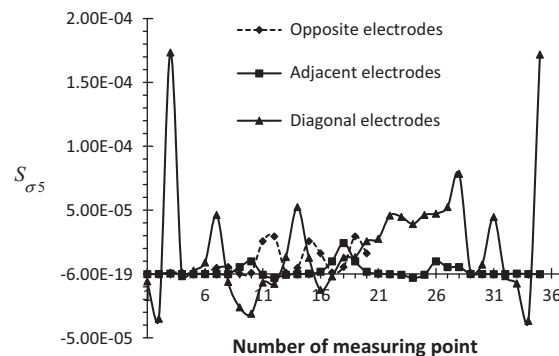
5.2. Identification

The identification of the electrical conductivity based on the results of the forward problem was presented, and the effect of some parameters on the identification was studied. For the measurements needed in the identification, in the first case, the exact voltages (U_{exact}) which are defined as voltages calculated from the forward problem using the exact values of the electrical conductivity ($\sigma_{exact} = 5$ S/m), was used.

(a) Electrical conductivity (σ_2)

(b) Electrical conductivity (σ_1)

(c) Electrical conductivity (σ_5)

Figure 8 Evolution of the sensitivity to electrical conductivity (comparison between 3 strategies of measure).

In the second section, for the measurements values (U_m), noisy simulated voltages were obtained by adding a relative error ζ to exact tensions

$$U_m = U_{exact} + \zeta.U_{exact}$$

5.2.1. Identification with exact voltage

Fig. 9 represents the identification of electrical conductivities ($\sigma_1 \ldots \sigma_5$) using exact voltage in the case of heterogeneous medium. It is clear that for different chosen initial value of the electrical conductivity (σ^0), the convergence of the Levenberg–Marquardt method was obtained. According to the initial value, the conductivity increases or decreases until to reach the exact value. This was confirmed with different conductivities. This study highlights the estimation of conductivity which changes with respect to z.
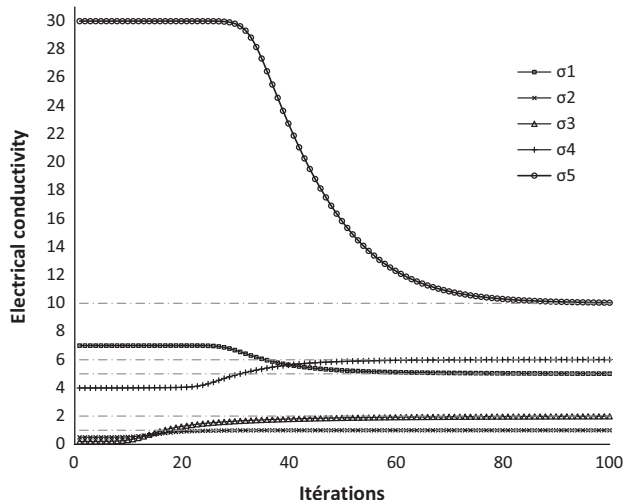
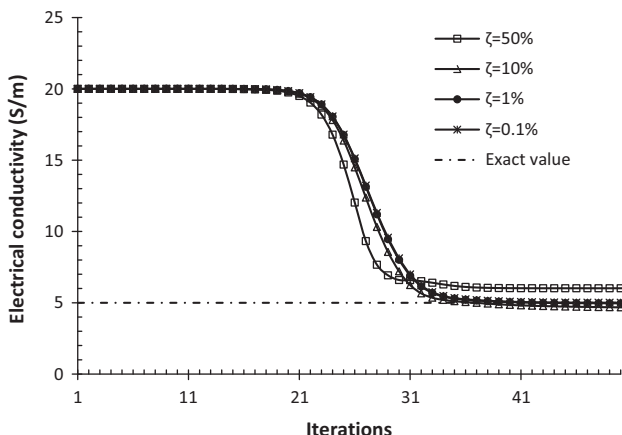**Figure 9** Identification of the electrical conductivity in a heterogeneous medium.

Figure 10 Identification of the electrical conductivity σ_2 with noisy simulated measures.
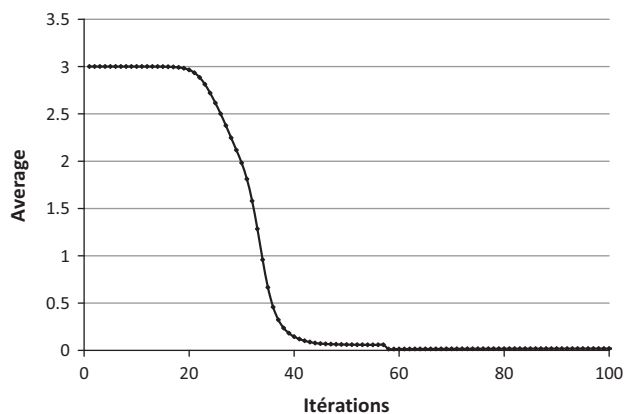

Figure 11 Error average.

5.2.2. Identification with noisy simulated voltage

The stability of the scheme with respect to the amount of noise added into the data (En Hong et al., 2015) is analyzed. As shown in Fig. 10, the identification of the electrical conductivity during iterations for different values of relative error ζ is represented. As illustrated in Table 1, an error of 21% is detected in the conductivity identification when the relative error ζ is 50% whereas it is 0.01% for an error ζ equal to 0.1%.

The effect of the measurements noise level on the identification precision was also studied in the case of heterogeneous medium. Estimation of different conductivities is illustrated in Table 2. It is clear that the identification is better for lower values of ζ. The estimation error is even higher when the measurement noise is higher for homogeneous and heterogeneous conductivity distribution.

The average (Fig. 11) and variance of the estimation errors are analyzed to prove the robustness and accuracy of the proposed method. The variance is calculated using the sum of squared deviations between the relative errors and the average E:

Table 1 Effect of the noise level of the measurements on the precision of the identification.

ζ (%)	50	10	1	0.1	0
$\sigma 1$ (S/m)	6.1392	4.5455	4.9505	4.9995	5
$\sigma 2$ (S/m)	6.0151	4.5455	4.9505	4.9995	5
$\sigma 3$ (S/m)	6.12	4.5455	4.9505	4.9995	5
$\sigma 4$ (S/m)	5.9925	4.5454	4.9505	4.9995	5
$\sigma 5$ (S/m)	6.066	4.5455	4.9505	4.9995	5
Error (%)	20–23	9	1	0.01	0

Table 2 Effect of the noise level of the measurements on the precision of the identification for heterogeneous medium.

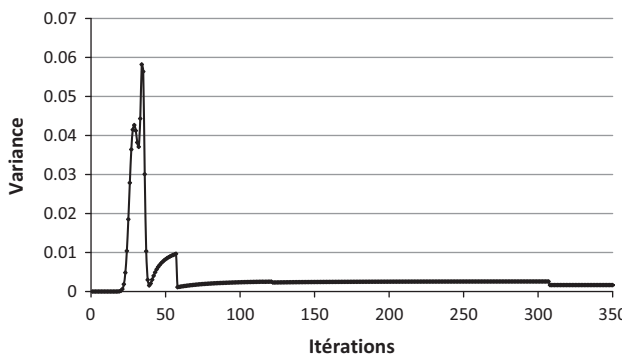| ζ (%)	50	10	1	0.1	0
$\sigma 1$ (S/m)	3.2391	4.5455	4.9505	4.995	5
$\sigma 2$ (S/m)	0.7365	0.9091	0.9901	0.999	1
$\sigma 3$ (S/m)	1.3352	1.8182	1.9802	1.998	2
$\sigma 4$ (S/m)	3.9474	5.4545	5.9406	5.994	6
$\sigma 5$ (S/m)	6.7779	9.0909	9.901	9.99	10
Error (%)	26–35	9	1	0.1	0

Figure 12 Variance.

$$Var(error) = \frac{1}{n}\sum(error - E)^2$$

As shown in Fig. 12, at the end of iterations, the variance achieved zero which indicates that all values are identical. Small changes in variance are noted in the middle, which sign that the values are close to each other.

6. Conclusion

An inverse method for electrical resistance tomography has been developed. The Levenberg–Marquardt method was used to solve the inverse problem, with the aim of identifying the electrical conductivity distribution necessary to determine the concentration and the fraction of the suspension. The resolution of the Laplace equation using the quadrupole method applied to the electrical fields, allowed to determine the electrical tension distribution. A sensitivity analysis was performed, which allowed to locate the positions and the measurement strategy containing the best information on the electrical property, and the identification of injection electrode position. The convergence of the Levenberg–Marquardt method depends mainly on the initial estimate parameter and the Levenberg–Marquardt parameter. The robustness of the developed algorithm was investigated by the identification of the conductivity with noisy simulated measures.

References

Abdullah, M.Z., Dyakowski, T., Dickin, F.J., Willams, R.A., 1993. Observation of hydrocyclone seperator dynamics using resistive electrical impedance tomography. In: Proc. European concerted Action on Process Tomography, Karlsruche. UMIST, Manchester, pp. 93–96.

Batsale, J., Maillet, D., Degiovanni, A., 1994. Extension de la méthode des quadripôles thermiques à l'aide de transformations intégrales—calcul du transfert thermique au travers d'un défaut plan bidimensional. Int. J. Heat Mass Transf. 37 (1), 111–127.

Binley, A., Shaw, B., Henry-Poulter, S., 1996. Flow pathways in porous media: electrical resistance tomography and dye staining image verification. Meas. Sci. Technol. 7 (3), 384–390.

Bond, J., Cullivanu, J.C., Climpson, N., Faulkes, I., Jia, X., Kostuch, J.A., Payton, D., Wang, M., Wang, S.J., West, R.M., Williams, R.A., 1999. Industrial monitoring of hydrocyclone operation using electrical resistance tomography, In: Proceedings of 1st World Congress on Industrial Process Tomography, Buxton, UK, pp. 102–107.

Brebbia, C., Dominguez, J., Tassoulas, J., 1991. Boundary elements: an introductory course. J. Appl. Mech. 58 (3), 860.

Cilliers, J., Wang, M., Neethling, S., 1999. Measuring flowing foam density distributions using ERT. 1st World Congress on Industrial Process Tomography, pp. 108–112.

Dahlin, T., 1996. 2D resistivity surveying for environmental and engineering applications. First Break 14 (7), 275–283.

Dahlin, T., 2001. The development of DC resistivity imaging techniques. Comput. Geosci. 27 (9), 1019–1029.

Dahlin, T., Zhou, B., 2004. A numerical comparison of 2D resistivity imaging with 10 electrode arrays. Geophys. Prospect. 52 (5), 379–398.

Das, M., Guven, I., Madenci, E., 2006. Coupled BEM and FEM analysis of functionally graded material layers. J. Therm. Stresses 29 (3), 263–287.

Degiovanni, A., 1988. Conduction dans un "mur" multicouche avec sources: extension de la notion de quadripole. Int. J. Heat Mass Transf. 31 (3), 553–557.

Dickin, F., Wang, M., 1996. Electrical resistance tomography for process applications. Meas. Sci. Technol. 7 (3), 247–260.

Dong, F., Jiang, Z., Qiao, X., Xu, L., 2003. Application of electrical resistance tomography to two-phase pipe flow parameters measurement. Flow Meas. Instrum. 14 (4–5), 183–192.

En Hong, L., Hj. Abdul Rahim, R., Ahmad, A., Md. Yunus, M., Aba, K., Pei Ling, L., Wahid, H., Ahmad, N., Abd Shaib, M., Abdul Wahab, Y., Aw, S., Rahiman, H., Zakaria, Z., 2015. Fundamental sensor development in electrical resistance tomography. J. Teknologi 73 (6).

Fguiri, A., Daouas, N., Radhouani, M., Ben Aissia, H., 2013. Inverse analysis for the determination of heat transfer coefficient. Revue canadienne de physique 91 (12), 1034–1043.

Fudym, O., Ladevie, B., Batsale, J., 2002. A seminumerical approach for heat diffusion in heterogeneous media: one extension of the analytical quadrupole method. Numer. Heat Transfer, Part B 42 (4), 325–348.

Fudym, O., Pradère, C., Batsale, J., 2007. An analytical two-temperature model for convection–diffusion in multilayered systems: application to the thermal characterization of microchannel reactors. Chem. Eng. Sci. 62 (15), 4054–4064.

Giguère, R., Fradette, L., Mignon, D., Tanguy, P., 2008a. ERT algorithms for quantitative concentration measurement of multiphase flows. Chem. Eng. J. 141 (1–3), 305–317.

Giguère, R., Fradette, L., Mignon, D., Tanguy, P., 2008b. Characterization of slurry flow regime transitions by ERT. Chem. Eng. Res. Des. 86 (9), 989–996.

Hallaji, M., Pour-Ghaz, M., 2014. A new sensing skin for qualitative damage detection in concrete elements: rapid difference imaging with electrical resistance tomography. NDT and E Int. 68, 13–21.

Hua, P., Woo, E.J., Webster, J.G., Tompkins, W.J., 1987. Effect of the measurement method on noise handling and image quality of ERT imaging. In: Proceedings of the 9th annual conference of the IEEE engineering in medicine and biology society. Institute of Electrical and Electronics Engineers, pp. 1429–1430.

Khambampati, A., Lee, B., Kim, K., Kim, S., 2012. An analytical boundary element integral approach to track the boundary of a moving cavity using electrical impedance tomography. Meas. Sci. Technol. 23 (3), 035401.

Kim, M., Kim, K., Kim, S., Lee, K., 2004. Reconstruction algorithm of electrical impedance tomography for particle concentration distribution in suspension. Korean J. Chem. Eng. 21 (2), 352–357.

Kim, S., Wang, R., Khambampati, A., Lee, B., Kim, K., 2014. An improved boundary distributed source method for electrical resistance tomography forward problem. Eng. Anal. Boundary Elem. 44, 185–192.

Kourunen, J., Rinne, A., Saloheimo, K., Heikkinen, L.M., 2008. Electrical tomography imaging of flotation process in a mechanical flotation cell. 5th International Symposium on Process Tomography.

Lehikoinen, A., Laakkonen, P., Vauhkonen, M., Rinne, A., Saloheimo, K., Lähteenmäki, S., 2011. Measuring flotation process using probe sensor based on 3d electrical resistance tomography. In: Proc of Flotation.

Liu, Q., Han, Y., Zhang, X., 2014. An image reconstruction algorithm based on Bayesian theorem for electrical resistance tomography. Optik – Int. J. Light Electron Opt. 125 (20), 6090–6097.

Lucas, G., Cory, J., Waterfall, R., Loh, W., Dickin, F., 1999. Measurement of the solids volume fraction and velocity distributions in solids–liquid flows using dual-plane electrical resistance tomography. Flow Meas. Instrum. 10 (4), 249–258.

Ma, Y., Zheng, Z., Xu, L., Liu, X., Wu, Y., 2001. Application of electrical resistance tomography system to monitor gas/liquid two-phase flow in a horizontal pipe. Flow Meas. Instrum. 12 (4), 259–265.

Mann, R., Williams, R.A., Dyakowski, T., Dickin, F.J., Edwards, R.B., 1995. Development of mixing models using resistance tomography. In: Scott, D.M., Williams, R.A. (Eds.), Frontiers in Industrial Process Tomography. Engineering Foundation, p. 324.

Moré, J.J., 1978. The Levenberg-Marquardt algorithm: implementation and theory. Numer. Anal., 105–116.

Nissinen, A., Lehikoinen, A., Mononen, M., Lähteenmäki, S., Vauhkonen, M., 2014. Estimation of the bubble size and bubble loading in a flotation froth using electrical resistance tomography. Miner. Eng. 69, 1–12.

Normi, V., Lehikoinen, A., Mononen, M., Rintamäki, J., Maksimainen, T., Luukkanen, S., Vauhkonen, M., 2009. Predicting collapse of the solid content in a column. In: Proc of Flotation.

Pailhes, J., Pradere, C., Battaglia, J., Toutain, J., Kusiak, A., Aregba, A., Batsale, J., 2012. Thermal quadrupole method with internal heat sources. Int. J. Therm. Sci. 53, 49–55.

Ren, S., Xu, Y., Tan, C., Dong, F., 2013. Reconstructing the geometric configuration of three dimensional interface using electrical capacitance tomography. Int. J. Numer. Meth. Eng. 96 (10), 628–644.

Reunanen, J., Mononen, M., Vauhkonen, M., Lehikoinen, A., Kaipio, J.P., 2011. Machine learning approach for locating phase interfaces using conductivity probes. Inverse Prob. Sci. Eng. 19, 879–902.

Rosales, R., Martínez-Pagan, P., Faz, A., Moreno-Cornejo, J., 2012. Environmental monitoring using electrical resistivity tomography (ERT) in the subsoil of three former petrol stations in SE of Spain. Water Air Soil Pollut. 223 (7), 3757–3773.

Sasaki, Y., 1992. Resolution of resistivity tomography inferred from numerical simulation. Geophys. Prospect. 40 (4), 453–463.

Seagar, A., Barber, D., Brown, B., 1987. Electrical impedance imaging. IEE Proc. A Phys. Sci. Meas. Instrum. Manage. Educ. Rev. UK 134 (2), 201–210.

Tapp, H., 2000. Status and applications of microelectrical resistance tomography. Chem. Eng. J. 77 (1–2), 119–125.

Tossavainen, O., Vauhkonen, M., Kolehmainen, V., 2007. A three-dimensional shape estimation approach for tracking of phase interfaces in sedimentation processes using electrical impedance tomography. Meas. Sci. Technol. 18 (5), 1413–1424.

Wang, M., 2000. Measurements of gas–liquid mixing in a stirred vessel using electrical resistance tomography (ERT). Chem. Eng. J. 77 (1–2), 93–98.

Wang, M., Dorward, A., Vlaey, D., Mann, R., 1999. Measurements of gas-liquid mixing in a stirred vessel using electrical resistance tomography (ERT). 1st World Congress on Industrial Process Tomography, Buxton, pp. 78–83.

Williams, R.A., Dickin, F.J., Gutierrez, A., Beck, M.S., Wang, M., Ilyas, O.M., Dyakowski, T., 1995. Monitoring cyclone performance using resistance tomography. In: Scott, D.M., Williams, R. A. (Eds.), Frontiers in Industrial Process Tomography. Engineering Foundation, pp. 261–274.

Xie, C.G., Reinecke, N., Beck, M.S., Mewes, D., Williams, R.A., 1995. Electrical tomography techniques for process engineering applications. Biochem. Eng. J. 56 (3), 127–133.

Xu, Y., Dong, F., 2010. Galerkin boundary element method for the forward problem of ERT. Flow Meas. Instrum. 21 (3), 172–177.

Xu, Y., Dong, F., Tan, C., 2010. Electrical resistance tomography for locating inclusions using analytical boundary element integrals and their partial derivatives. Eng. Anal. Boundary Elem. 34 (10), 876–883.

Zhou, B., Dahlin, T., 2003. Properties and effects of measurement errors on 2D resistivity imaging surveying. NSG 1 (24), 105–117.